IJMGE
Int. J. Min. & Geo-Eng.
Vol.48, No.1, June 2014, pp. 11-30.

Assessing the Performance of Statistical-structural and Geostatistical Methods in Estimating the 3D Distribution of the Uniaxial Compressive Strength Parameter in the Sarcheshmeh Porphyry Copper Deposit

Mahboubeh Pishbin *, Nader Fathianpour

Department of Mining Engineering, Isfahan University of Technology, Isfahan, Iran

Received 25 November 2013; Received in revised form 5 February 2014; Accepted 10 May 2014
**Corresponding author: m.pishbin@mi.iut.ac.ir*

Abstract

The uniaxial compressive strength (UCS) of intact rocks is an important geotechnical parameter required for designing geotechnical and mining engineering projects. Obtaining accurate estimates of the rock mass UCS parameter throughout a 3D geological model of the deposit is vital for determining optimum rock slope stability, designing new exploratory and blast boreholes, mine planning, optimizing the production schedule and even designing the crusher's feed size. The main objective of this paper is to select the preferred estimator of the UCS parameter based on accuracy performance using all the available geological-geotechnical data at the Sarcheshmeh copper deposit, located 160 km southwest of Kerman City, in south-eastern Iran. In this paper, an attempt is made to estimate the spatial distribution of the UCS parameter using commonly-used statistical-structural and geostatistical methods. In order to achieve the aim of the current study, the UCS parameter was measured along with other qualitative geological properties, including the rock type, weathering, alteration type and intensity of core samples taken from 647 boreholes. The 3D distribution of the UCS parameter is obtained using different algorithms including statistical-structural (the nearest-neighbour technique), linear (ordinary Kriging) and nonlinear (indicator Kriging) geostatistical methods. After estimating the UCS parameter at block centres using the above-mentioned methods, the performance of each method is compared and validated through 21 set aside borehole data. The assessment of selecting best estimator of UCS parameter is based on scatter plots of the observed versus estimated data plus the root mean square error (RMSE) statistics of the differences between observed and estimated values for 21 set aside borehole data. Finally, due to the special characteristics of the UCS spatial variability, it is concluded that the nearest-neighbour method is the most appropriate method for estimating the UCS parameter in porphyry copper deposits.

Keywords: *indicator Kriging, nearest-neighbour, ordinary Kriging, sarcheshmeh copper deposit, uniaxial compressive strength (UCS).*

1. Introduction

Generally, site characterization starts with the process of refining the engineering geology properties throughout the spatial domain of any facility installation. It involves assessing data adequacy and accuracy, data interpretation and integration, and setting up a conceptual model. In areas where the geological setting is well known, site characterization may be a straightforward procedure. However, where weathering and alterations have intensively degraded rock strength, site development and design may require extra attention in establishing rock slope stabilities. Studying the spatial influence of weathering or alteration on rock masses through certain rock parameters is, therefore, useful in developing a standard rock mass description. This would enable us to have an even more refined rock classification based on the actual geology under investigation [1]. The uniaxial compressive strength (UCS) is one of the most important intact rock parameters used for the purpose of design in a variety of engineering applications, such as tunnel excavation, rock slopes, foundations, etc. Since it has a significant relationship with the rock type, the alteration and weathering type and intensity, it is used as an input parameter in some rock mass classification systems. Obtaining accurate rock mass UCS estimates throughout a 3D geological model of deposit is vital for determining the optimum rock slope stability, designing new exploratory and blast boreholes, mine planning, optimizing the production schedule and even designing the crusher's feed size.

In order to increase the accuracy of estimating geotechnical parameters, a number of methods, such as simple and multiple regression and geostatistics have already been employed. These methods have been applied for estimating geotechnical parameters such as the UCS with some success [1-13]. For example, Diamantis et al. (2009) investigated the relationships among the physical, dynamical and mechanical properties of intact rocks, and attempted to derive reliable, empirical approaches for estimating the UCS parameter. The results were statistically described and analysed using the method of least squares regression [9]. Basu and Kamran (2010) used a linear regression model to obtain a correlation between the UCS and point load index (I_S) measurements [11].

Ayalew et al. (2002) employed geostatistics first to determine the spatial variability of the rock quality designation (RQD), which has a direct relationship with weathering; next, they used geostatistics to carry out the estimation of RQD values based on the ordinary Kriging method [1]. Raspa et al. (2008) combined techniques of multivariate statistics and geostatistics and compared them to evaluate the estimation methods of the geotechnical parameters, with special reference to the drained friction angle from the direct shear test (φ') [12].

In addition, several traditional and widely-used estimation methods have been described by a number of researchers, including Patterson (1959), King et al. (1982), Annels (1991) and Stone and Dunn (1994) [14-17]. These procedures include polygonal (such as nearest-neighbour), triangular, regular and random stratified grid, inverse distance weighting and contouring methods. The nearest-neighbour method is a popular method routinely employed in many fields of the earth sciences, including geotechnical engineering.

The aim of this study is to find the most efficient and geologically consistent method for estimating the UCS parameter at regular grid locations throughout a 3D geological model of a porphyry copper deposit using common estimation and interpolation methods.

2. Methodology

The UCS values available to the current study, along with other qualitative geological properties including rock type, the weathering and alteration type and intensity were measured on core samples taken from 647 boreholes at the Sarcheshmeh copper deposit. In this study, the UCS parameter is estimated at the centre of each block in the 3D geological solid model with a block size of 12.5×12.5×6.25 metres throughout the ore body's extent. To find the best method for estimating the UCS parameter in terms of accuracy and consistent with the governing geology, the performance of different widely-used estimators or interpolators is assessed. Primarily, the statistical-structural (nearest-neighbour technique) and linear (ordinary Kriging) and nonlinear (indicator Kriging) geostatistical methods are employed to determine the spatial variability of the UCS parameter, which often shows a direct relationship with rock type, weathering and alteration type and intensity. The results could discriminate the predefined 67 different classes based on rock type, weathering and alteration intensities with respect to their estimated UCS values throughout the Sarcheshmeh copper deposit. Following the estimation of the UCS parameter at block centres using the above-mentioned methods, the performance of each method is compared and validated by employing 21 set aside borehole data. The assessment of selecting best estimator of UCS parameter is based on scatter plots of the observed versus estimated data plus the root mean square error (RMSE) statistics of the differences between observed and estimated values of 21 set aside borehole data. The methodology used in the present study is shown in Figure 1.

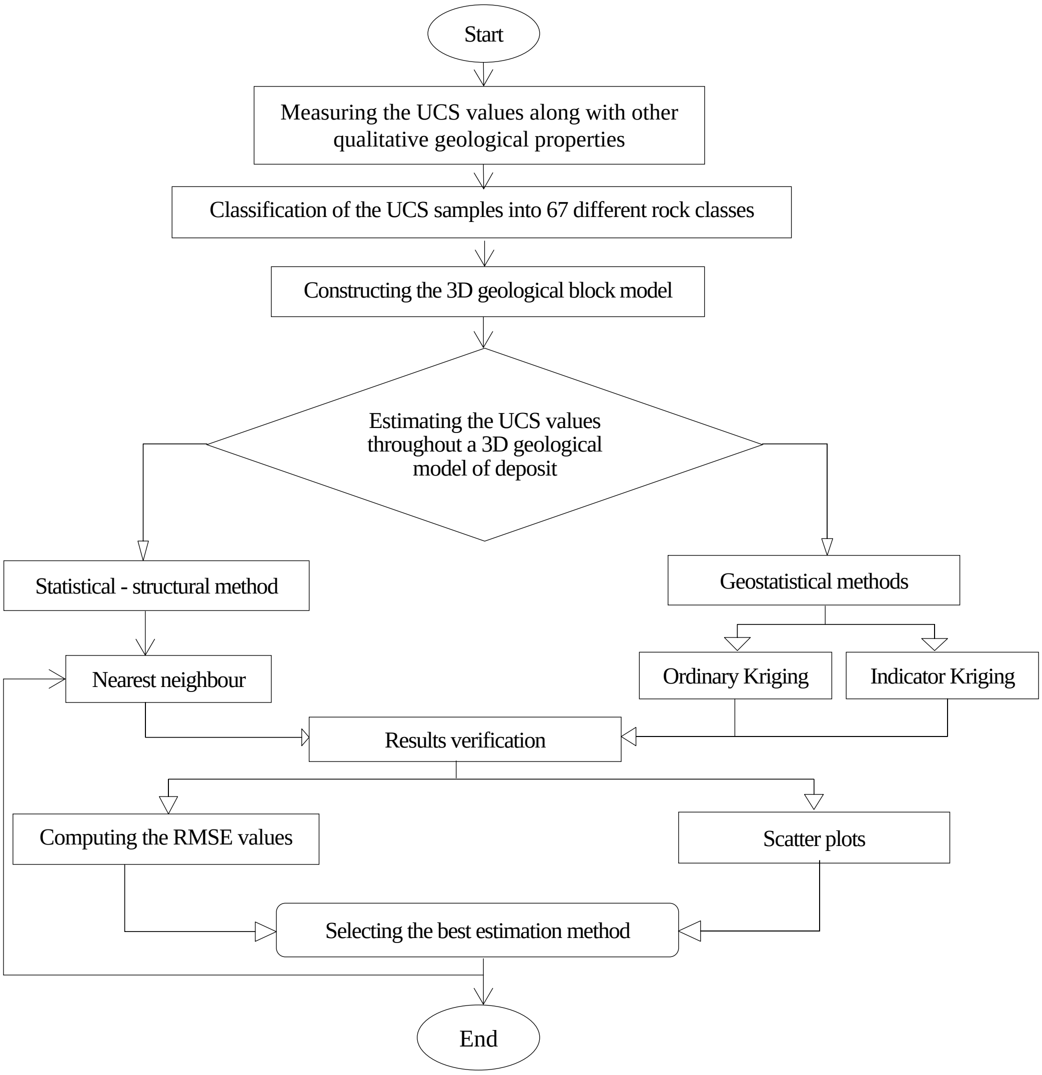

Fig. 1. Proposed workflow for selecting the best method in estimating the 3D distribution of the UCS parameter.

2.1. Ordinary Kriging and Indicator Kriging Methods

Geostatistics includes several estimation techniques commonly known as 'Kriging' that can be used for estimating spatially distributed variables in certain unsampled locations. The most commonly-used Kriging methods are ordinary Kriging (OK) method and the indicator Kriging (IK) method. The OK method is used to estimate the values of a variable of interest at an unsampled location using a variogram model interpreted from all the spatially distributed samples throughout a deposit and the data located in its local search ellipsoid. Under the assumption that the region is second-order stationary, ordinary block kriging implicitly evaluates the mean in a moving neighborhood in a manner that minimizes the estimation variance. However, if the block average values are to be estimated, then the OK method is adapted in such a way so as to average the discretized sub-block Kriging values [18, 19].

In geostatistics, nonlinear interpolation involves estimating the conditional expectation and conditional distribution of the variable distribution of interest at locations within the region of interest as opposed to estimating a single average variable. When the variable distributions of interest have a near-normal shape, a linear estimator is ideal. However, when the variable distribution of interest is highly skewed or else contains a mixture of populations, the underlying assumption of ordinary estimation methods can be invalidated. In these cases, a nonlinear estimation method can more appropriately handle these more complex distributions. There are many nonlinear geostatistical estimation methods which can be used to make local (panel-by-panel) estimates of distributions of interest. The IK method is one such nonlinear method routinely employed in many fields of the earth sciences, including geotechnical engineering. IK is performed on binary indicator transformed values of the variables for one or more thresholds of interest. The continuity of the indicators for each threshold is modelled as by an indicator variogram as the structural function. The indicators are then estimated using OK to give the probability estimate of exceeding or not exceeding the thresholds of interest. The IK estimate of each single indicator lies within the interval [0, 1] and can be interpreted as:

1. The probability that the value of the variable exceeds the indicator threshold, or;
2. The proportion of the block or panel above the specified cut-off of the data (point) support.

Indicators methods are also useful for characterizing the spatial variability of categorical variables [18, 19].

2.2. The Nearest-neighbour Method

In this section, the fundamental base of the popular interpolating method, namely the nearest-neighbour (NN), is discussed first. In the NN method, the centre of the block is assigned the value of the nearest sample, where the nearest distance is defined as a transformed or anisotropic distance which takes account of any anisotropy structure in the spatial distribution of the variable. The NN method does not make use of weighting sample values during the course of estimation [18, 20].

3. Application to the Study Area

3.1. Introducing the Sarcheshmeh Copper Deposit

The Sarcheshmeh porphyry copper deposit is located 160 km southwest of Kerman City, in south-eastern Iran. The entire mineralization is embedded in a volcanic belt intruded by a number of intrusive stocks known as the 'Uromiyeh-Dokhtar zone'. The average elevation of the deposit is 2,600 meters above sea level and its centre is at a latitude of 29°56′N and a longitude of 55°52′E. The geographical position of Sarcheshmeh copper mine is shown in Fig. 2. The ore body is oval-shaped with a long dimension of about 2,300 metres and a width of about 1,200 metres.

3.2. Geological Setting

The porphyry copper mineralization at Sarcheshmeh is associated with a granodioritic stock intruded into a folded and faulted early tertiary volcano-sedimentary series. The volcanic rocks in the Sarcheshmeh area are principally fine-grained andesite porphyries. The magmatism at the Sarcheshmeh deposit is believed to be a multi-stage intrusion process. The main intrusion - the Sarcheshmeh porphyry - is cut by a sub-volcanic body, the so-called 'late fine porphyry', and by several felsic dikes. The mineralogy of these dikes and their time relationship to mineralization allow them to be grouped into intra-mineralization (early hornblende porphyry), late-mineralization (late hornblende porphyry) and post-mineralization (feldspar porphyry and biotite porphyry) dikes. In the andesitic wall rocks, three different zones are observed which are concentric to the potassic and phyllic altered Sarcheshmeh porphyry (the stock). The internal zone closest to the stock is characterized by strong biotitic and weak phyllic alteration, with a thickness from 50 to 400 m (at 2,400 m elevation). This zone passes progressively into the next zone, whose external boundary closely follows the line of the 0.4% Cu cut-off grade. This intermediate zone is characterized by weak biotitic and strong phyllic alterations. Its thickness at 2,400 m elevation varies from 50 to 150 m. The thickness of an external altered andesitic zone (propylitic) is very large, extending towards unaltered rocks in all directions [21]. Three classes of alteration and weathering intensities are defined for the different rock types designated by 1 to 3, denoting slight (S), moderate (M) and high (H) intensities, respectively. The lithology and alteration plans of the Sarcheshmeh copper deposit at 2,200 m elevation are shown in Figures 3 and 4.

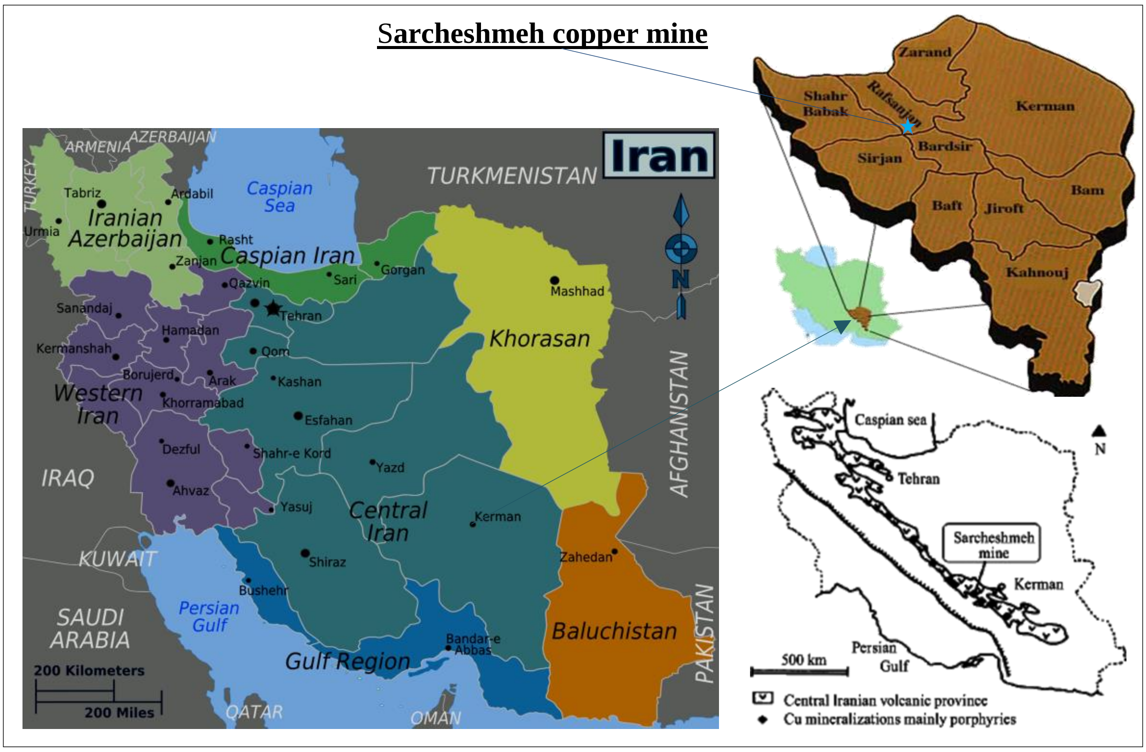

Fig. 2. Geographical position of the Sarcheshmeh copper mine [modified after 21].

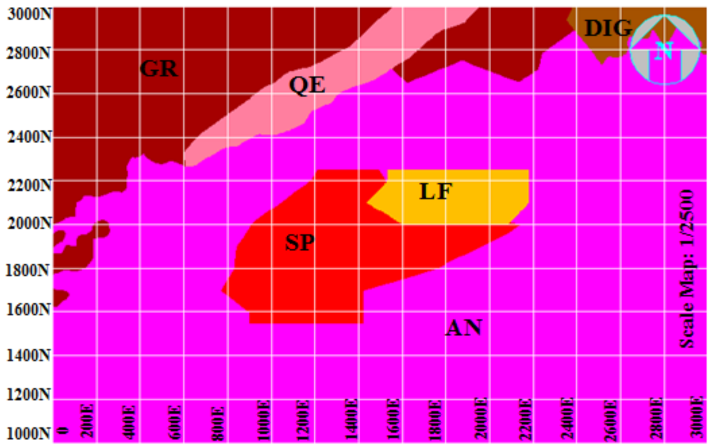

Fig. 3. Plan of the lithology distribution at 2,200 m elevation in the Sarcheshmeh copper deposit (AN: Andesite, SP: the Sarcheshmeh porphyry, LF: Late the fine porphyry, GR: granodiorite, QE: the quartz eye porphyry, DIG: dacite ignimbrite) [22].

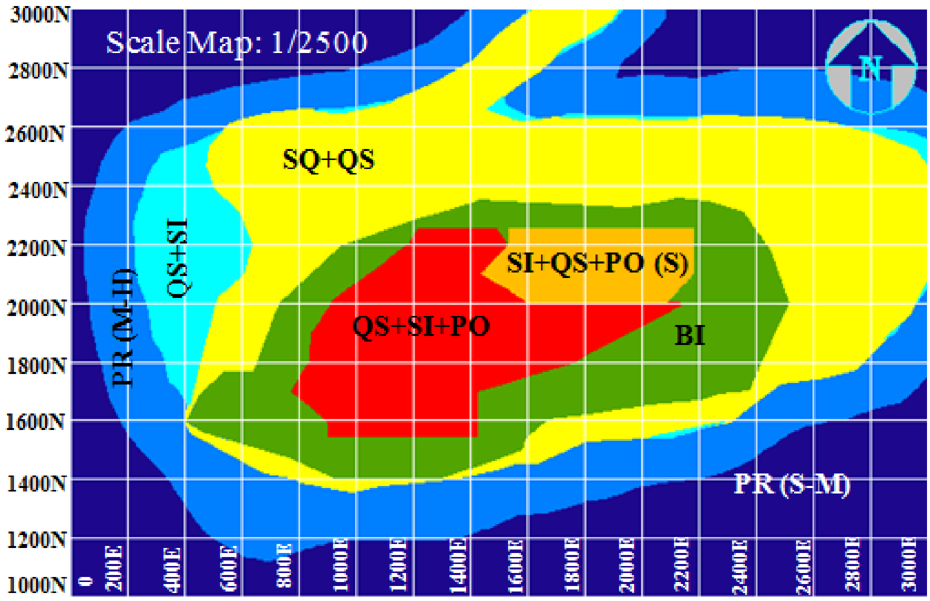

Fig. 4. Plan of rock alterations at 2,200 m elevation in the Sarcheshmeh copper deposit (PO: potassic, QS: quartz sericite, SQ: sericite quartz, SI: silicified, BI: biotite, PR: propylitic, S: slightly altered, M: moderately altered, H: highly altered) [22].

3.3. Data Preparation

In order to estimate the UCS parameter value at the centre of a regular grid of blocks, core samples taken along 647 boreholes encompassing 101,493 core sample data throughout the 3D extent of the deposit were employed. The procedure for measuring this rock strength parameter has been standardized by both the ISRM and ASTM [23 and 24], so it is not re-stated in this paper.

Since the height of the actual working bench designed for the mining procedure is five metres, we have chosen the compositing size to be five metres as well. Finally, 23,988 composited UCS values were used for interpolation and 1,632 composited core sample data taken from 21 set-aside boreholes covering both the 3D spatial estimation space and the full-range of the UCS variation were deployed for cross-validation. The histograms of the entirety and the testing data of the UCS are shown in Figures 5a and 5b, respectively.

In the first step, it was necessary to establish the relationship between the rock mass UCS parameter with the rock type, alteration or weathering type and intensity throughout the deposit extent. Since it is expected that the observed UCS parameter values will show a strong association with the governing geology characterized by the lithology type, alteration and weathering type and intensities, it can be clearly seen that the stronger the alteration and weathering, the lower the UCS values (and vice versa), except for those cases where the alterations have been associated with silicification. Thus, the existing relationship between the UCS and engineering geology parameters, incorporating rock type, weathering and alteration type and intensity in the estimation process is expected to result in a better estimation of the rock mass UCS parameter throughout the deposit's 3D extent. As a first step, the UCS values along with other qualitative geological parameters, including rock type, weathering and alteration type and intensity, were collected. The different rock types, weathering and alteration types and intensities observed throughout the 3D extent of the deposit are given in Table 1.

Through such classification, 67 categories of UCS values based on rock properties were diagnosed. The amount of data and average UCS values of the main rock units designated by the associated intensity and type of rock weathering and alteration are summarized in Table 2.

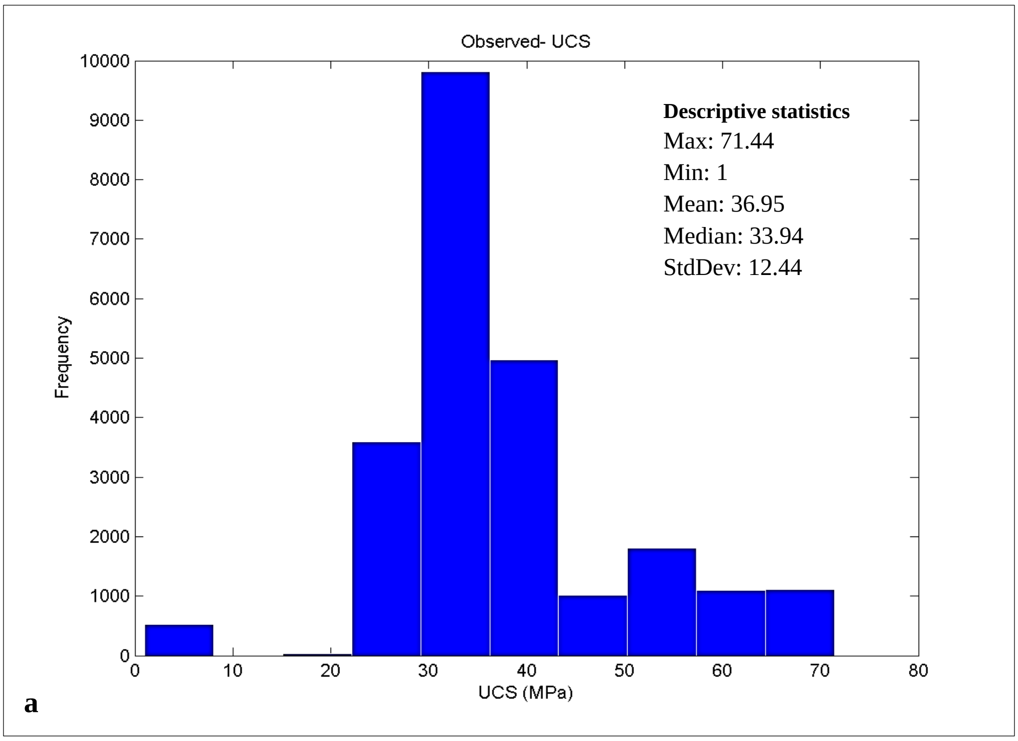

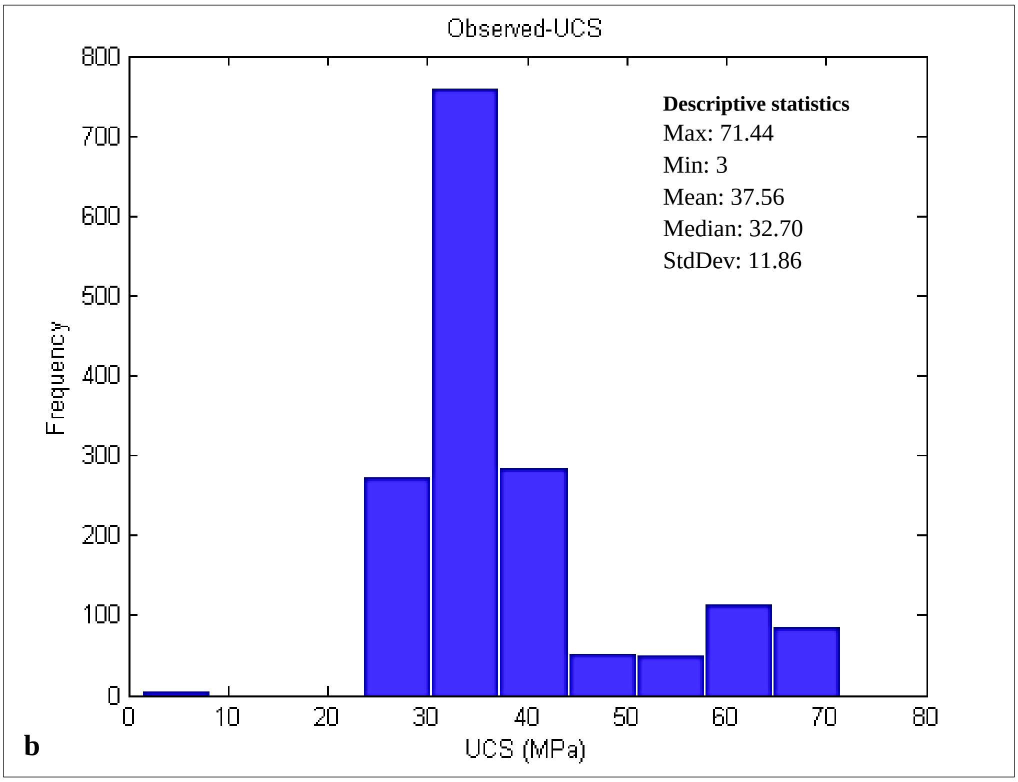

Fig. 5. Histograms of: a) the entirety, and b) the testing UCS datasets.

Table 1. Observed rock types, weathering and alteration types and intensities in the Sarcheshmeh deposit.

Alteration type	Rock type	Weathering or alteration intensity
Propylitic (PR)	Andesite (AN)	1(Slightly Weathering or Alteration (SW or SA))
Quartz Sericite (QS)	Granodiorite (GR)	2 (Moderately Weathering or Alteration (MW or MA))
Sericite Quartz (SQ)	Sarcheshmeh Porphyry (SP)	3 (Highly Weathering or Alteration (HW or HA))
Silicified (SI)	Late Fine porphyry (LF)	
Biotite (BI)	Quartz Eye porphyry (QE)	
Potassic (PO)	Biotit Dyke (BD)	
Argillic (AR)	Hornblende Dyke (HD)	
	Feldspar Dyke (FD)	

Table 2. Amount of data and average UCS values of the main rock units designated by the associated intensity and type of rock weathering and alteration in the study area.

Rock class	UCS (MPa)	Number	Rock class	UCS (MPa)	Number	Rock class	UCS (MPa)	Number
QE-QS-2	35.32	713	SP-SI-3	30	2368	BD-W-1	57	892
QE-QS-3	26.71	587	SP-SQ-2	36.37	868	BD-W-2	31.45	676
QE-SI-1	39.9	142	SP-SQ-3	27.51	702	BD-W-3	25.6	38
QE-SI-2	31	351	SP-PO-2	35.6	615	AN-PR-1	52.42	1113
QE-SQ-3	27.51	30	GR-PR-1	58.33	201	AN-PR-2	38.64	1357
LF-QS-1	59	5578	GR-PR-2	45.52	37	AN-PR-3	33.24	35
LF-QS-2	45.8	1359	GR-PR-3	26.46	34	AN-QS-1	45.43	671
LF-QS-3	40.15	35	GR-QS-2	26	1749	AN-QS-2	33.94	13434
LF-SI-2	40	31	GR-SQ-2	46.97	129	AN-QS-3	25.55	4522
LF-SI-3	34.44	30	GR-SQ-3	27.31	153	AN-BI-1	50.2	91
LF-SQ-2	34.7	46	GR-SI-2	32.1	151	AN-BI-2	31.9	2261
LF-SQ-3	26.24	34	GR-SI-3	25	31	AN-BI-3	26.17	7770
LF-PO-1	34.3	372	HD-W-1	71.44	6545	AN-SQ-2	32.7	7138
LF-PO-2	32.14	291	HD-W-2	45.12	13306	AN-SQ-3	29.71	2945
SP-QS-1	32.6	123	HD-W-3	31.13	6052	AN-SI-2	32.72	1311
SP-QS-2	34.95	2663	FD-W-1	58.5	103	AN-SI-3	25.47	1822
SP-QS-3	55	4288	FD-W-2	37.64	471			
SP-Si-2	44.53	3883	FD-W-3	26.24	100			

3.4. Generation of Estimation Methods

3.4.1. Estimating the UCS Parameter Using the OK Method

The most common geostatistical tool for modelling spatial dependencies is the semi-variogram. The semi-variogram γ(h) is a function describing the degree of spatial dependency of a spatial random field or stochastic process Z(x). The semi-variogram formulates the difference between any two sample values as a function of their distance [18]. An omnidirectional semi-variogram of the UCS variable for a segment size of 5 m is shown in Fig. 6. It is worth noting that the UCS classification in the pre-processing step was only used to estimate the core sample UCS parameter along boreholes based on an established linear relationship with the point load data, and it is not addressed in the current paper. In the presence of anisotropy, the continuity of the UCS spatial distribution varies with the direction. This is usually represented by a 3D ellipsoid where the lengths and directions of the three orthogonal axes of the ellipsoid describe the spatial continuity and orientation. In the present study, the geometric anisotropy parameters were estimated using the principal component analysis (PCA) method. Directional semi-variograms of the UCS variable for a segment size of 5 m are shown in Figs. 7a, 7b and 7c.

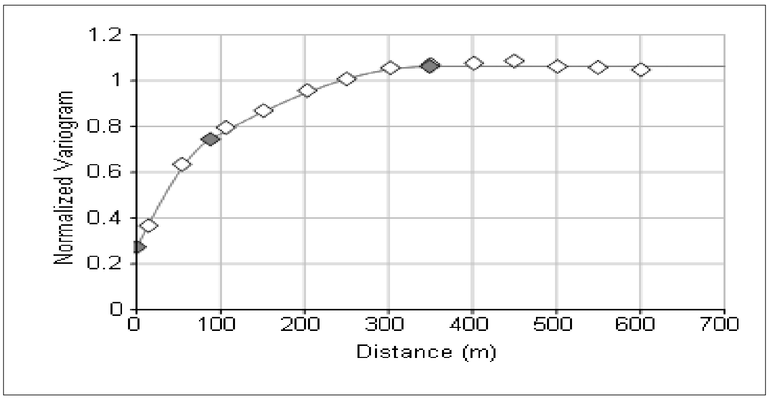

Fig. 6. Experimental omnidirectional semi-variogram overlaid by its fitted spherical model.

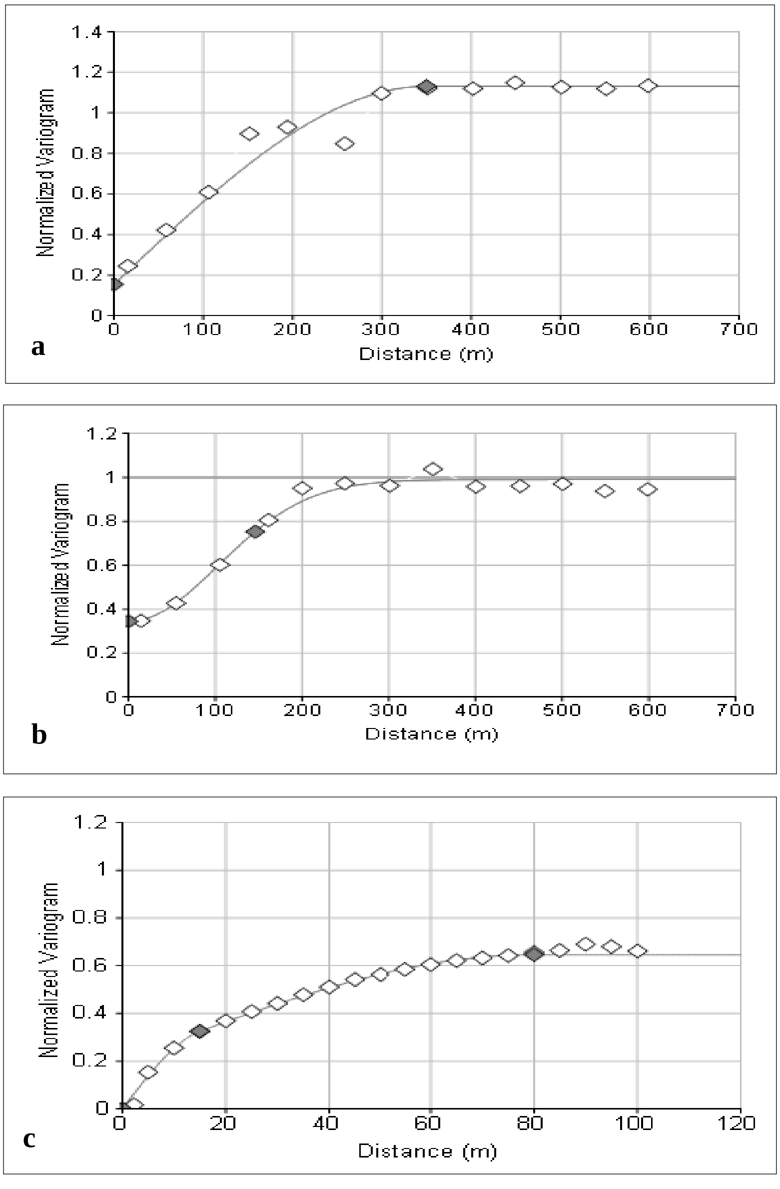

Fig. 7. Experimental semi-variograms of the UCS values overlaid by: a, c) their fitted spherical model, and b) their fitted Gaussian model in three different directions.

In order to improve the estimation procedure, the data were employed in three different search volumes enabling the coverage of the entire deposit's spatial domain. The standardized semi-variogram model parameters are shown in Table 3.

Table 3. Standardized variogram model parameters.

Semi-Variogram		Model Type	Nugget Effect	Spatial Variance	Range (m)
Omni-Directional (Nested Structures)	Structure 1	Spherical	0.274	0.284	88
	Structure 2	Spherical		0.505	350
X		Spherical	0.141	0.811	350
Y		Gaussian	0.345	0.645	147
Z (Nested Structures)	Structure 1	Spherical	0.000	0.202	15
	Structure 2	Spherical		0.444	80

The experimental variogram in Figure 7c clearly shows two nested structures - one at a smaller scale (about 15 m) and the other at a larger scale (about 80 m). It was decided to model and use both the large- and small-scale components of the variogram. Thus, the large-scale structure (structure two) was overlaid on top of the small-scale structure (structure one). However, it should be noted that, due to a lack of strong spatial continuity at the border of different rock units where the UCS parameter may vary abruptly (sharp changes of UCS values between adjacent blocks in different zones), the variogram models are inappropriate, causing less accurate estimates to be obtained by the OK algorithm. Despite such evident weakness, the OK method is used for 3D UCS modelling in the case study of the Sarcheshmeh copper ore deposit. Before performing Kriging estimations, it is important to assess the quality of the estimation by conducting a series of cross-validation tests. After fixing all the neighbourhood parameters, a cross-validation test is conducted using the experimental semi-variogram models. All the computations obtaining OK results are carried out using well-known 3D geostatistical modules of GSLIB employing appropriate anisotropic parameter-setting. The goodness-of-fit of the results is analysed using cross-validation. The histogram of the observed minus the estimated data is shown in Fig. 8, which closely follows a normal distribution. The mean of the estimation error is nearly equal to 0, which proves the unbiasedness of the OK estimates. In addition, the scatter plot of the observed versus the estimated data is shown in Figure 9.

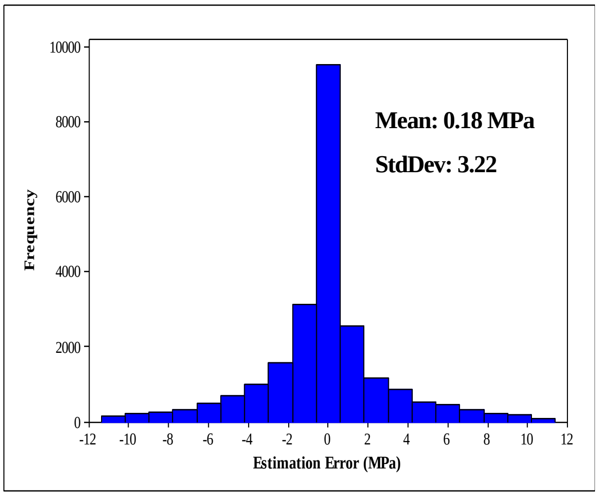

Fig. 8. Histograms of the estimation errors using the OK method.

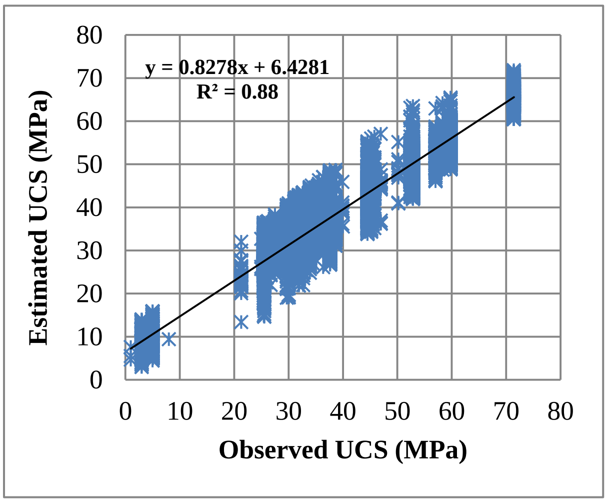

Fig. 9. Scatter plots of the observed data versus the estimated data using the OK method.

3.4.2. Estimating the UCS Parameter Using the IK Method

Since the UCS data are composed of different populations - resulting in a multi-modal distribution - the IK approach was selected as an appropriate nonlinear estimation method for estimating the UCS parameter. In this study, ten thresholds are used to obtain an adequate discretization of the conditional distributions. The selection of these 10 thresholds were based on adequately sampling the full distribution of the UCS values, comprising changes between different populations and- in particular- adequately characterizing the high and low UCS populations. The conditional cumulative distribution function (CCDF) model provides information about the range of UCS values as well as the corresponding frequency probabilities (Fig. 10). The ten threshold values correspond to the eight deciles in the CCDF distribution and two additional thresholds at the quantiles of 0.025 and 0.95. These extreme values will help in characterizing the high and low values, minimizing the extrapolation errors at these end limits. As can be seen from Figure 10, the threshold values at the CCDF values of 0.3 to 0.4 and 0.6 to 0.7 are equal, so only one of each was selected. Table 4 shows the threshold values and proportions that fall below that CCDF threshold value.

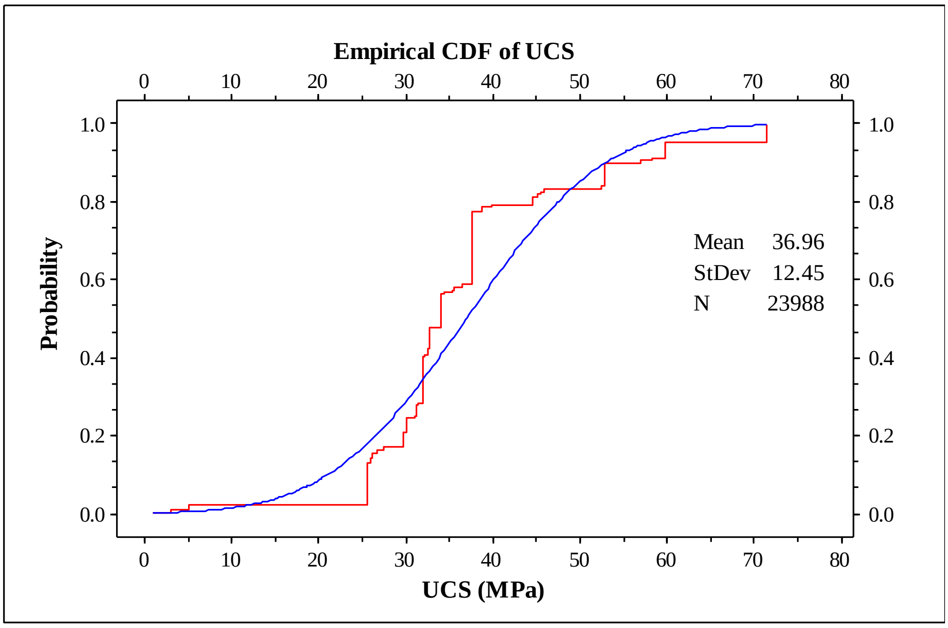

Fig. 10. Cumulative distribution function (CDF) model for determining threshold values.

In the current study, the geometric anisotropy parameters were estimated using the PCA method. The experimental variograms for all the thresholds in the vertical direction clearly show two nested structures, one at the smaller scale and the other at the larger scale. It was decided to model and use of both large- and small-scale components of the variogram. Thus, the large-scale structure (structure two) was added to the small-scale structure (structure one). Table 4 shows the parameters for the models fitted to the experimental variograms.

Before performing the Kriging estimations, it is important to assess the quality of the estimation by conducting a series of cross-validation tests. After fixing all the neighbourhood parameters, a cross-validation test was conducted using the experimental semi-variogram models. The goodness-of-fit of the results was analysed using cross-validation. The histograms of the observed minus the estimated data obtained by applying the E-type method on the IK probabilities is shown in Fig. 11, which closely follows a normal distribution. The mean of the estimation error is nearly equal to 0, which proves the unbiasedness of the IK estimates. In addition, the scatter plot of the observed versus the estimated data is shown in Figure 12.

Table 4. Standardized indicator variogram model parameters for defined threshold values.

CCDF	Cut off (MPa)	Semi-Variogram		Model Type	Nugget Effect	Spatial Variance	Range (m)
0.025	**8**	Omni-Directional (Nested Structures)	Structure 1	Spherical	0.186	0.570	70
			Structure 2	Spherical		0.276	250
		X		Spherical	0.068	0.957	250
		Y		Spherical	0.068	0.957	200
		Z (Nested Structures)	Structure 1	Spherical	0.089	0.009	15
			Structure 2	Spherical		0.548	40
0.1	**25.55**	Omni-Directional (Nested Structures)	Structure 1	Spherical	0.193	0.451	65
			Structure 2	Spherical		0.285	150
		X		Spherical	0.225	0.704	150
		Y		Spherical	0.175	0.725	115
		Z (Nested Structures)	Structure 1	Spherical	0.089	0.132	10
			Structure 2	Spherical		0.607	65
0.2	**29.71**	Omni-Directional (Nested Structures)	Structure 1	Spherical	0.161	0.379	65
			Structure 2	Spherical		0.317	150
		X		Spherical	0.221	0.640	150
		Y		Spherical	0.207	0.639	110
		Z (Nested Structures)	Structure 1	Spherical	0.075	0.089	15
			Structure 2	Spherical		0.611	65
0.3 0.4	**31.9**	Omni-Directional (Nested Structures)	Structure 1	Spherical	0.232	0.370	65
			Structure 2	Spherical		0.359	250
		X		Spherical	0.364	0.603	250
		Y		Spherical	0.357	0.582	200
		Z (Nested Structures)	Structure 1	Spherical	0.100	0.148	15
			Structure 2	Spherical		0.498	65
0.5	**33.94**	Omni-Directional (Nested Structures)	Structure 1	Spherical	0.235	0.375	75
			Structure 2	Spherical		0.364	250
		X		Spherical	0.367	0.608	250
		Y		Spherical	0.360	0.587	200
		Z (Nested Structures)	Structure 1	Spherical	0.110	0.153	15
			Structure 2	Spherical		0.503	75
0.6 0.7	**37.64**	Omni-Directional (Nested Structures)	Structure 1	Spherical	0.264	0.278	88
			Structure 2	Spherical		0.526	350
		X		Spherical	0.375	0.661	350
		Y		Spherical	0.396	0.558	250
		Z (Nested Structures)	Structure 1	Spherical	0.079	0.206	15
			Structure 2	Spherical		0.428	80
0.8	**44.53**	Omni-Directional (Nested Structures)	Structure 1	Spherical	0.275	0.277	88
			Structure 2	Spherical		0.544	350
		X		Spherical	0.400	0.579	250
		Y		Spherical	0.383	0.687	350
		Z (Nested Structures)	Structure 1	Spherical	0.075	0.226	15
			Structure 2	Spherical		0.383	80
0.9	**52.9**	Omni-Directional (Nested Structures)	Structure 1	Spherical	0.304	0.224	75
			Structure 2	Spherical		0.548	340
		X		Spherical	0.446	0.633	340
		Y		Spherical	0.425	0.567	250
		Z (Nested Structures)	Structure 1	Spherical	0.121	0.219	15
			Structure 2	Spherical		0.380	75
0.95	**59.8**	Omni-Directional (Nested Structures)	Structure 1	Spherical	0.450	0.136	75
			Structure 2	Spherical		0.500	280
		X		Spherical	0.682	0.385	280
		Y		Spherical	0.671	0.333	200
		Z (Nested Structures)	Structure 1	Spherical	0.179	0.245	15
			Structure 2	Spherical		0.398	60
1.0	**71.44**	Omni-Directional (Nested Structures)	Structure 1	Spherical	0.732	0.001	88
			Structure 2	Spherical		0.321	270
		X		Spherical	0.782	0.272	270
		Y		Spherical	0.782	0.207	200
		Z (Nested Structures)	Structure 1	Spherical	0.689	0.045	15
			Structure 2	Spherical		0.095	60

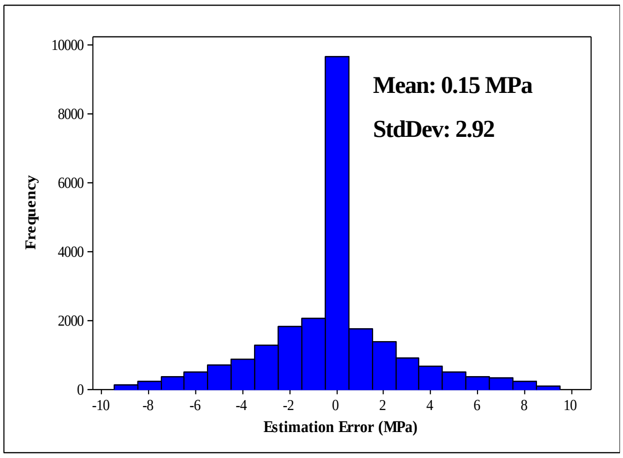

Fig. 11. Histograms of the estimation errors using the IK method.

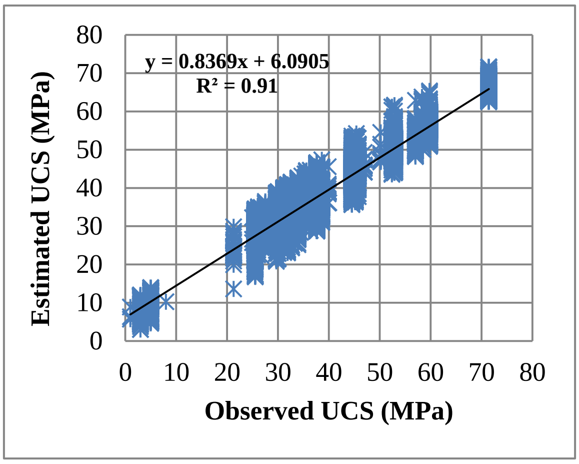

Fig. 12. Scatter plots of the observed data versus the estimated data using the IK method.

3.4.3. Estimating the UCS Parameter Using the NN Method

In this section, the most popular interpolating method- namely NN - is used for estimating the UCS parameter. The distances from the sample to the block centre are calculated based on an anisotropy ellipsoid (which is defined identically to the search ellipsoid parameters used in the OK method). Since the UCS variability is closely associated with the structural and lithological variations throughout the 3D deposit extent, it is therefore expected that obtain better estimates of the UCS parameter would be obtained if geological information were to be used in the estimation process. For this reason, the NN algorithm (which takes into account the anisotropic structure of the governing geology in the estimation process) has provided some benefit, as is seen in the results outlined below. The goodness-of-fit of the different estimators is analysed using cross-validation. The histograms of the observed minus the estimated data obtained by the NN method are shown in Figure 13 and they closely follow a normal distribution. In addition, a scatter plot of the observed versus the estimated data is shown in Figure 14.

As is seen from Figure 13, the histogram of the errors - defined as the difference between the estimated and the true values - associated with the NN method is focused on zero, showing that the exactness of most estimated values (although there are a few overestimated values caused by sharp contrasts with narrow hornblende dykes that have the highest UCS values among the other rock units).

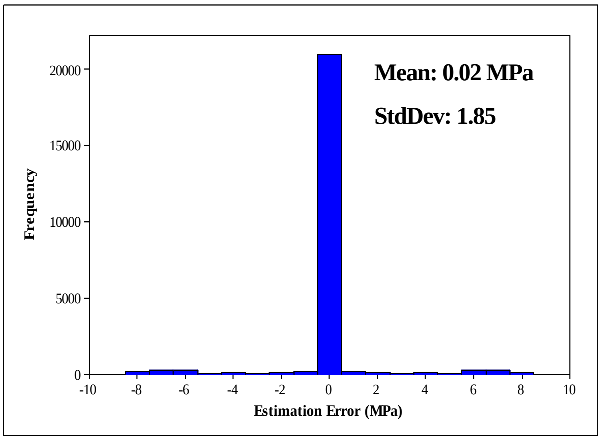

Fig. 13. Histogram of the estimation errors using the NN method.

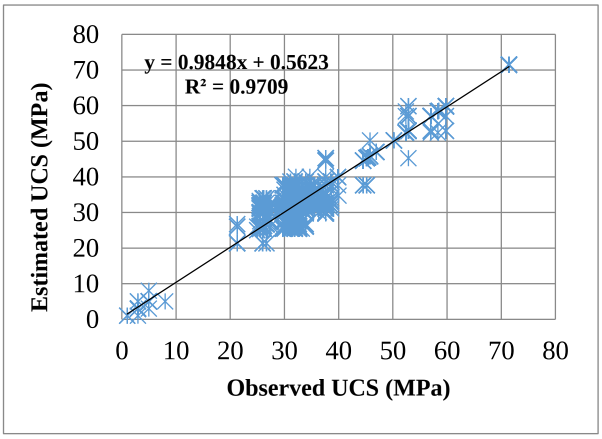

Fig. 14. Scatter plots of the observed data versus the estimated data using the NN method.

3.5. Construction of 3D Input Geological Models

In this section, a geological block model is constructed based on the wireframes (a wireframe is a surface or 3D volume formed by linked points together to form triangles) and drill hole data. The model contains an upper surface constraint defined by the surface topography and uses the ore body volume wireframe to control the internal constraints between ore and waste.

A solid model is composed of a number of connected 3D blocks, each of which has a number of attributes, such as type of rock, alterations and dykes. A parent block is the largest block allowed in the model. The size of these blocks is selected based on several factors, such as the drill hole spacing, the mining method (bench height) and the ore deposit's geological settings. Sub-blocking allows the subdivision of the parent blocks into smaller blocks for better fir with the wireframe dimensions.

In this study, 3D solid models of alteration, lithology and dykes are created with a block size of 12.5×12.5×6.25 metres and a sub-block size of 3×3×3 metres throughout the ore body extent. The final 3D geological solid model is created by combining these models together. It is worth noting that the geological solid model has been built taking into account borehole data. This final geological model is used as input for the NN, OK and IK estimators in estimating the UCS parameter at the centre of the blocks.

3.6. Estimation of the UCS Parameter from the 3D Input Geological Model

Once cross-validation has been carried out and all the parameters are optimized, the next step is the estimation of the UCS parameter using the NN, OK and IK methods at the centre of each block in the 3D geological solid model with a block size of 12.5×12.5×6.25 metres throughout the ore body extent. The objective of the interpolation process is to provide a 3D geological solid model of the estimated UCS values which portrays the spatial distribution of the UCS values of weathered and altered rock masses throughout the study area.

3.7. Construction of the 3D UCS Models

Finally, 3D geological solid model of the estimated UCS values is constructed which portrays the spatial distribution of the UCS values of the weathered and altered rock masses throughout the study area. The estimated UCS values obtained by the NN, OK and IK methods on a plan of 2,200 metres height above sea level for visual assessment are shown in Figs. 15 to 17 (see Table 2 for comparison). It is worth noting that the highest UCS values shown on these plans correspond to the intruded intact hornblende dykes which are excluded from the geological map (Fig. 3).

3.8. Validating Models

There are many diagnostic statistics capable of evaluating the validity of any estimation when a value Z* is estimated from the values of a regionalized variable Z known at a number of locations. The mean, standard deviation and RMSE are among these statistics. It is well established that a zero RMSE denotes global unbiasedness in the estimation procedure.

After estimating the UCS parameter at the centre of each block in the 3D geological solid model using different methods, the obtained results and performance of each method are compared and validated employing 21 set-aside boreholes encompassing 1,632 core sample data covering the 3D estimation space and the full range of UCS variation (Fig. 5b). The location map of the above-mentioned 21 boreholes selected for validating the final derived models is shown in Figure 18.

The comparison of the results obtained by the above-mentioned methods is based on the RMSE of the differences between the observed and estimated values of 21 boreholes data. The results obtained by all the studied models are shown in Table 5 for comparison.

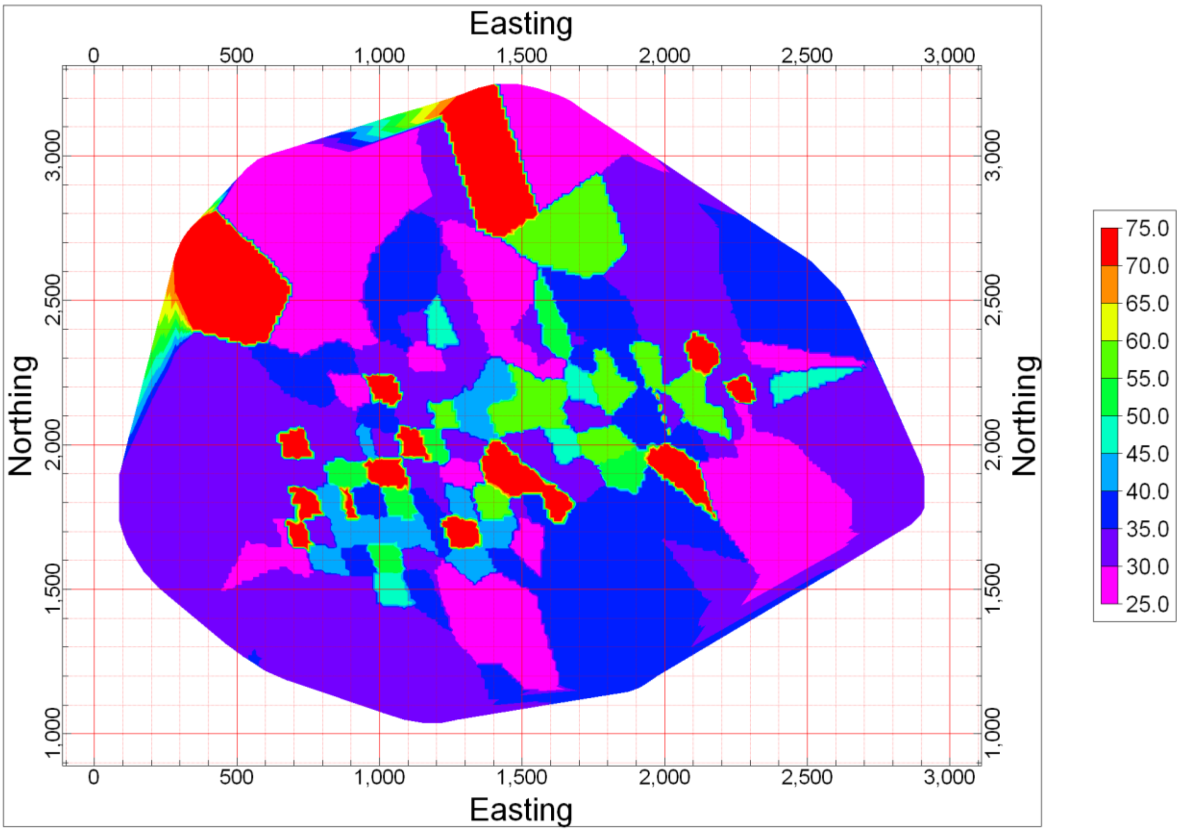

Fig. 15. Plan of the UCS estimates using the NN method at 2,200 m height above sea level.

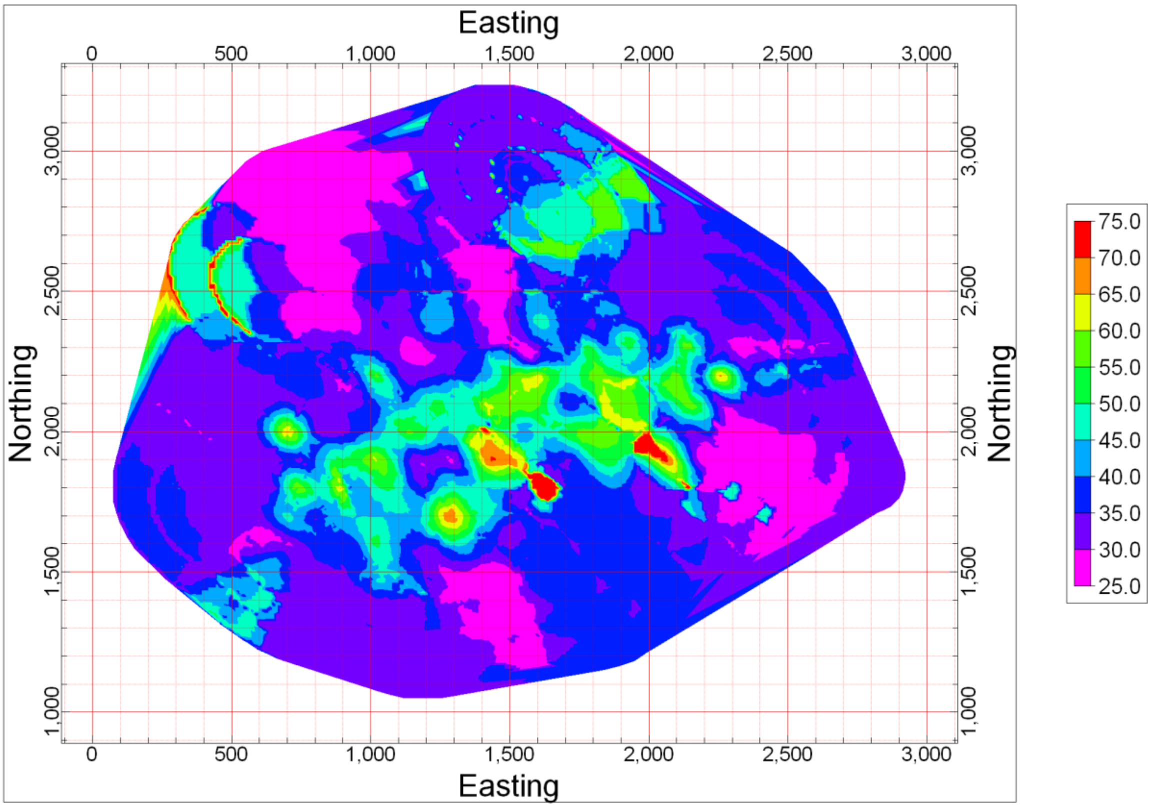

Fig. 16. Plan of the UCS estimates using the OK method at 2,200 m height above sea level.

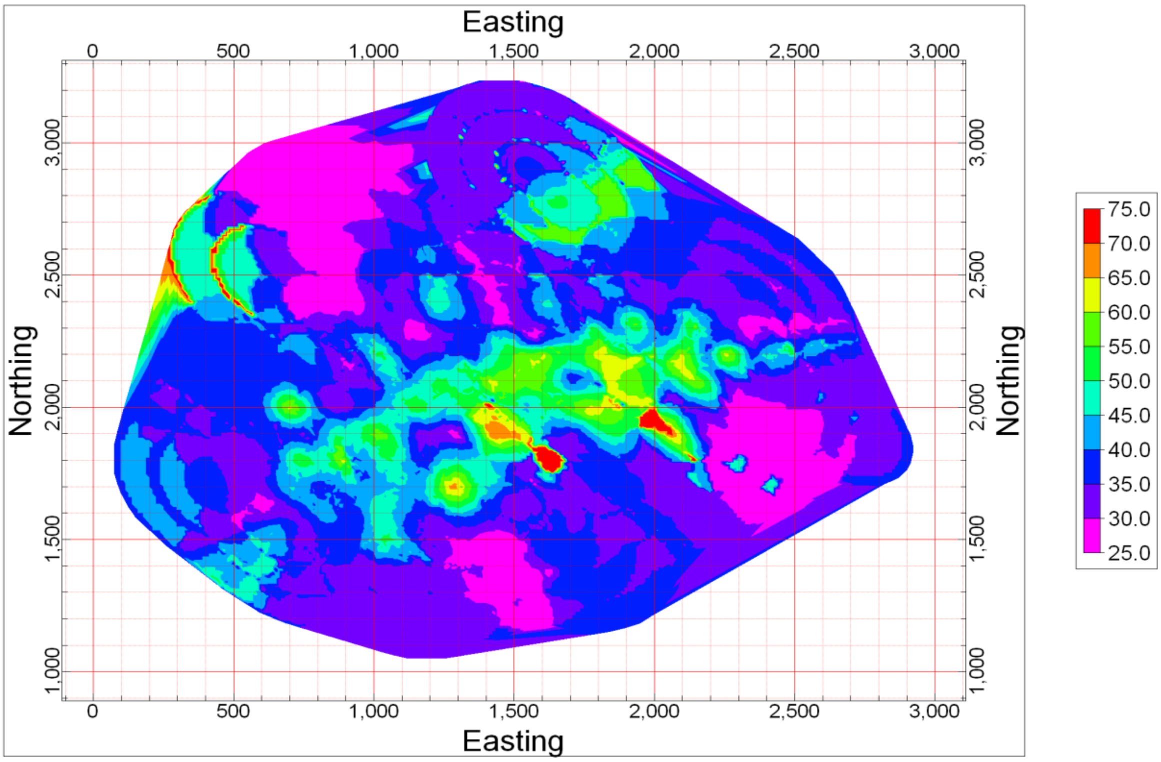

Fig. 17. Plan of the UCS estimates using the IK method at 2,200 m height above sea level.

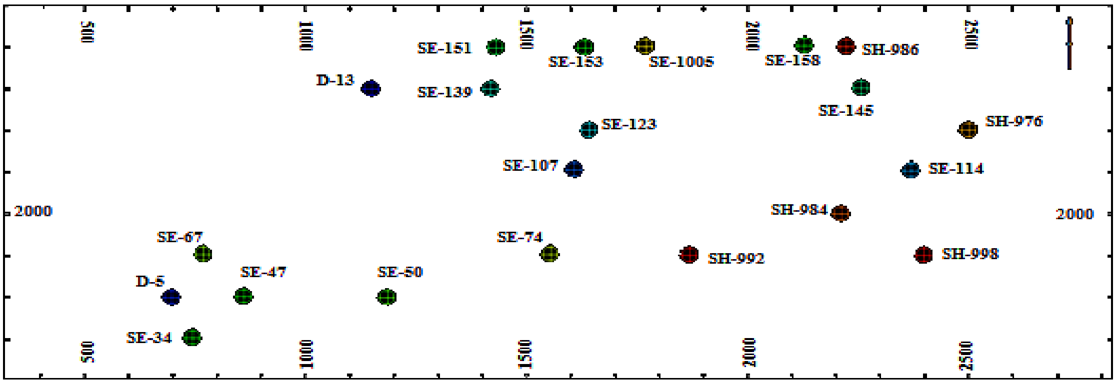

Fig. 18. Location map of 21 boreholes selected for validating the final derived models.

Table 5. The results obtained by different models.

Descriptive statistics	Observed UCS (MPa)	Estimated UCS (MPa) (NN)	Estimated UCS (MPa) (OK)	Estimated UCS (MPa) (IK)
Max	71.44	71.44	70.94	70.16
Min	3	3	10.02	11.97
Mean	37.56	37.16	37.05	37.50
StDev	11.86	12.34	9.82	9.37
RMSE	-	2.01	3.15	2.90

Based on the estimation error measure, the NN outperformed the other estimators; however, the superiority of the estimators is evaluated not only based on error statistics but also on consistency with the original data and the cross-validation of the estimated versus the observed data using tools like scatter plots. Finally, based on the cross-validation by means of the RMSE statistics and scatter plots, the NN is the most appropriate interpolation method for estimating the UCS parameter. The histograms of the observed minus the estimated data and the scatter plots of the estimated versus the observed data by NN method using testing data are shown in Figures 19 and 20, respectively. As is seen from Figure 19, the histogram of the errors -defined as the difference between the estimated and true values- associated with the NN method is focused on zero, meaning the exactness of most of the estimated values (although there are a few overestimated values caused by sharp contrasts with narrow hornblende dykes that have the highest UCS values among the other rock units). In contrast, the histogram of the estimate errors made by the OK and IK methods shows a wider distribution due to the contribution of all the neighbouring points in the estimation process. Furthermore, the estimated UCS values using the NN method show better agreement with the governing geology, both in terms of lithology, alteration and weathering, such that stronger alterations correspond with lower UCS values and vice versa (Fig. 15) (see Figs. 3 and 4 for comparison). Histograms of the estimated UCS values obtained by NN method using the entirety of the data and the testing data are shown in Figure 21. As can be seen in Figure 21, the histograms of the estimated UCS values obtained by the NN method show better agreement with the histograms of the observed UCS values (see Fig. 5 for comparison).

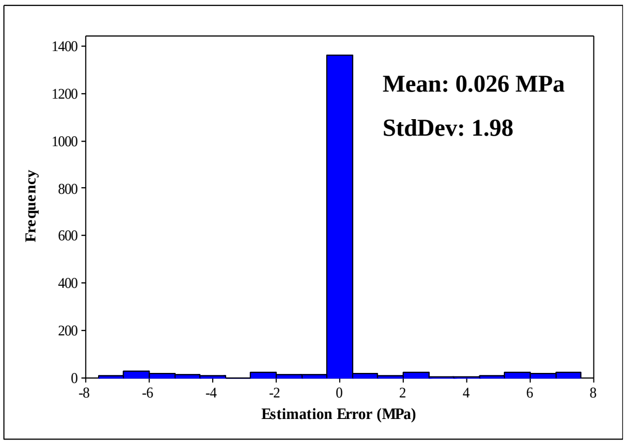

Fig. 19. Histogram of estimation errors obtained by the NN method using testing data.

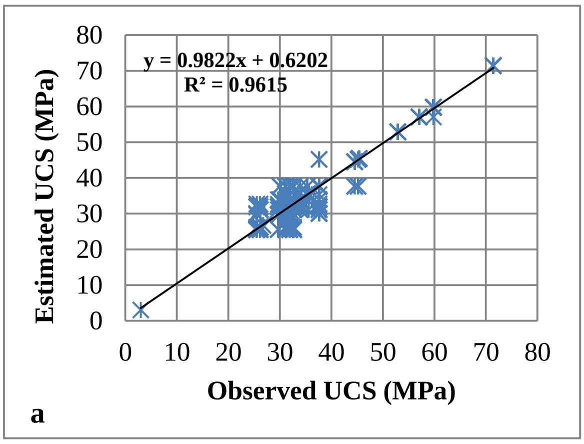

Fig. 20. Scatter plot of the observed testing data versus the estimated data using the NN method.

4. Conclusions

In the presented research, statistical-structural and geostatistical methods were employed to assess their capabilities in estimating the UCS parameter in terms of accuracy and consistency with engineering geology parameters in the Sarcheshmeh copper deposit. The relationship between the UCS and rock mass weathering and alterations were employed to improve the estimation of the UCS parameter. The UCS parameter was estimated at the block centres in the 3D geological solid model with a block size of 12.5×12.5×6.25 metres throughout the ore body extent incorporating engineering geology parameters in the estimation procedure. Common interpolating methods, including the NN, OK and IK methods are used to generate a 3D solid model of the estimated UCS values. The results show that the addition of geological information (a combination of lithology, weathering and alteration resulting in 67 rock class codes) into the predictor variables and the generalization of the UCS parameter through its relationship with a point-load index could significantly improve the estimation accuracy of the UCS parameter in different parts of the Sarcheshmeh copper deposit. Based on the comparison of the different methods, we can conclude that the superiority of the NN interpolating algorithm is due to the sharp UCS variation between the different rock units, on the one hand, and less variation inside the rock units on the other hand. Therefore, this reason physically explains why the NN method enhances the accuracy of the interpolation procedure, resulting in a tangible estimation error reduction.

Finally, it is concluded that, based on the cross-validation by means of the RMSE statistics for 21 set-aside borehole data and scatter plots, the NN is the most appropriate interpolation method for estimating the UCS parameter at the Sarcheshmeh site and similar porphyry copper deposits.

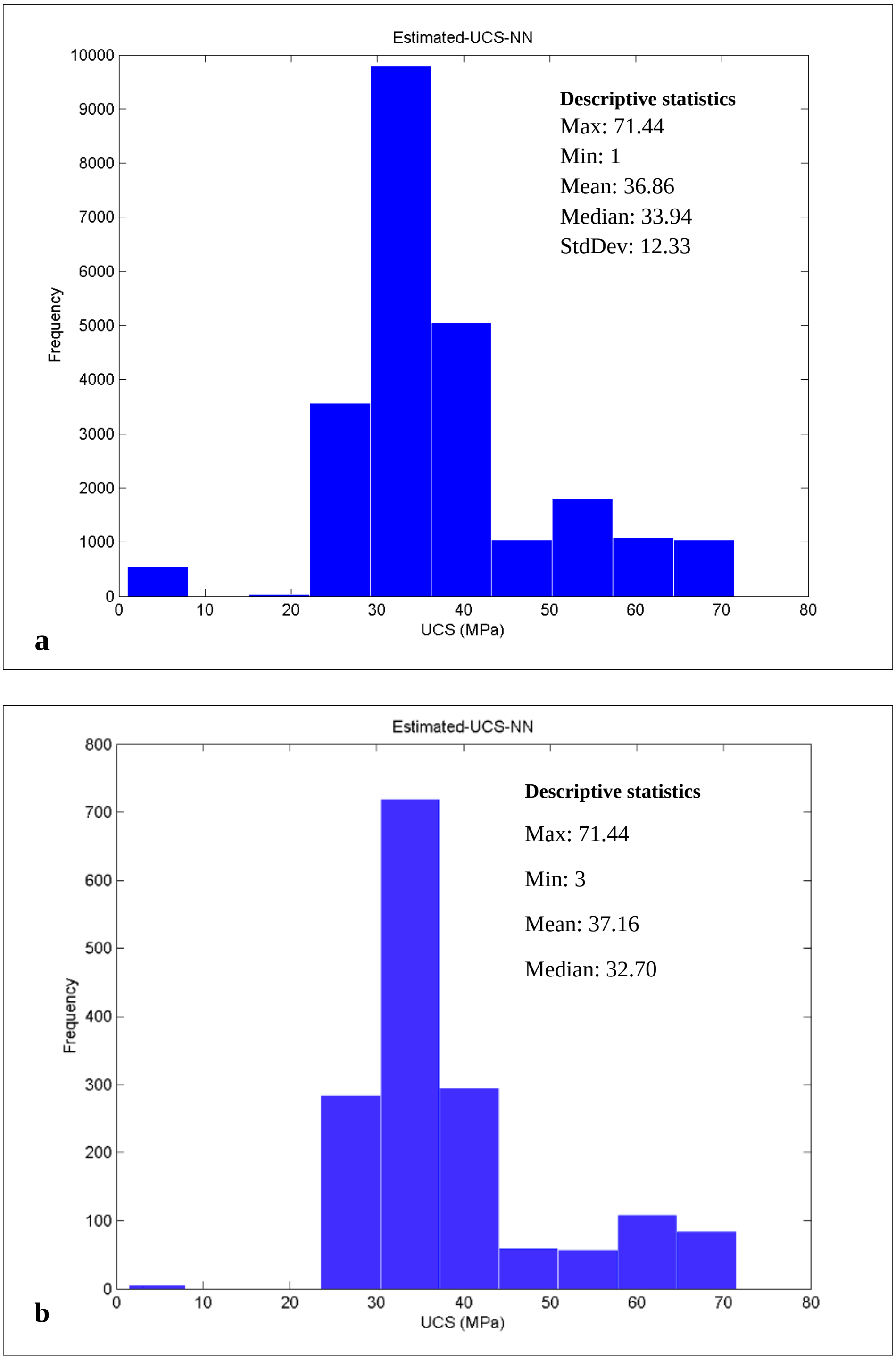

Fig. 21. Histogram of the estimated values obtained by the NN method using: a) the entirety of the data, and b) the testing data.

Acknowledgements

This work has been partially supported by the NICICO (National Iranian Copper Industrial Company). The authors would like to thank the mining research unit of the research and development division for their permission to utilize the data and present this paper. Furthermore, the authors would like to thank Morteza Asadipour, the chief geologist of the geotechnical department at Sarcheshmeh copper mine, who oversees exploration, drilling and testing programmes in the Sarcheshmeh copper mine and who helped us in preparing the data.

References

[1] Ayalew, L., Reik, G. and Busch, W. (2002). Characterizing weathered rock masses-a geostatistical approach. International Journal of Rock Mechanics and Mining Sciences, 39, pp. 105-114. PII: S1365-1609 (02) 00004–7.

[2] Kahraman, S. (2001). Evaluation of simple methods for assessing the uniaxial compressive strength of rock. International Journal of Rock Mechanics and Mining Science, 38, pp. 981–994. PII: S1365-1609 (01) 00039–9.

[3] Tsiambaos, G. and Sabatakakis, N. (2004). Considerations on strength of intact sedimentary rocks. Engineering Geology, 72, pp. 261- 273. http://dx.doi.org/ 10.1016/ j.enggeo. 2003.10.001.

[4] Fener, M., Kahraman, S., Bilgil, A. and Gunaydin, O. (2005). A comparative evaluation of indirect methods to estimate the compressive strength of rocks. Rock Mechanics and Rock Engineering, 38, pp. 329–343.

[5] Kahraman, S., Gunaydin, O. and Fener, M. (2005). The effect of porosity on the relation between uniaxial compressive strength and point load index. International Journal of Rock Mechanics and Mining Science, 42, pp. 584–589. http://dx.doi.org/ 10.1016/j.ijrmms.2005.02.004.

[6] Çobanoğlu, İ. and Çelik, S.B. (2008). Estimation of uniaxial compressive strength from point load strength, Schmidt hardness and P-wave velocity. Bulletin of Engineering Geology and the Environment, 67, pp. 491–498. http://dx.doi.org/10.1007/s10064-008-0158x.

[7] Kılıç, A. and Teymen, A. (2008). Determination of mechanical properties of rocks using simple Methods. Bulletin of Engineering Geology and the Environment, 67, pp. 237–244. http://dx.doi.org/ 10.1007/s10064-008-0128-3.

[8] Sabatakakis, N., Koukis, G., Tsiambaos, G. and Papanakli, S. (2008). Index properties and strength variation controlled by microstructure for sedimentary rocks. Engineering Geology, 97, pp. 80–90. http://dx.doi.org/10.1016/j.enggeo. 2007.12.004.

[9] Diamantis, K., Gartzos, E. and Migiros, G. (2009). Study on uniaxial compressive strength, point load strength index, dynamic and physical properties of serpentinites from central Greece: Test results and empirical relations. Engineering Geology, 108, pp. 199–207. http://dx.doi.org/ 10.1016/j.enggeo.2009.07.002.

[10] Kahraman, S. and Gunaydin, O. (2009). The effect of rock classes on the relation between uniaxial compressive strength and point load index. Bulletin of Engineering Geology and the Environment, 68, pp. 345–353. http://dx.doi.org/ 10.1007/s10064-009-0195-0.

[11] Basu, A. and Kamran, M. (2010). Point load test on schistose rocks and its applicability in predicting uniaxial compressive strength. International Journal of Rock Mechanics and Mining Sciences, 47, pp. 823-828. http://dx.doi.org/ 10.1016/ j.ijrmms.2010.04.006.

[12] Raspa, G., Moscatelli, M., Stigliano, F., Patera, A., Marconi, F., Folle, D., Vallone, R., Mancini, M., Cavinato, G.P., Milli, S. and Costa, J.F.C. (2008). Geotechnical characterization of the upper Pleistocene–Holocene alluvial deposits of Roma (Italy) by means of multivariate geostatistics: Cross-validation results. Engineering Geology, 101, pp. 251–268. http://dx.doi.org/ 10.1016/ j.enggeo.2008.06.007.

[13] Marache, A., Breysse, D., Piette, C. and Thierry, P. (2009). Geotechnical modeling at the city scale using statistical and geostatistical tools: The Pessac case (France). Engineering Geology, 107, pp. 67–76. doi:10.1016/j.enggeo.2009.04.003.

[14] Patterson, J.A. (1959). Estimating ore reserves follows logical steps. Engineering and Mining Journal, 160, pp. 111–115.

[15] King, H.F., McMahon, D.W. and Bujtor, G.J. (1982). A guide to the understanding of ore reserve estimation. Proceeding of the Australasian Institute of Mining and Metallurgy, 281, pp. 1-21.

[16] Annels, A. E. (1991). Mineral Deposit Evaluation: A Practical Approach. Chapman and Hall Publishers, London, 436 pp.

[17] Stone, J.G., and Dunn, P.G. (1994). Ore reserve estimates in the real world. Society of Economic Geologists, Special Publication, 15 pp.

[18] Webster, R. and Oliver, M. (2007). Geostatistics for Environmental Scientists. John Wiley & Sons, Ltd, Chichester, 332 pp.

[19] Badel, M., Angorani, S. and Shariat Panahi, M. (2011). The application of median indicator kriging and neural network in modeling mixed population in an iron ore deposit. Computers and Geosciences, 37, pp. 530–540. http://dx.doi.org/ 10.1016/ j.cageo.2010.07.009.

[20] Newland, J. (2009). A Guide to the Processes and Procedures Involved in Studio 3, Grade Estimation. United Kingdom, p. 61.

[21] Shahabpour, J. (2000). Some sulfide- silicate assemblages from the Sarcheshmeh porphyry copper deposit, Kerman, Iran. Iranian Journal of Science, 11, 1-10.

[22] Abdollahi, M. (2009). Alteration and lithology maps of Sarcheshmeh copper deposit. Report of Geological Studies of Sarcheshmeh Copper Deposit, Kerman, Iran, 177 pp [in Persian].

[23] ISRM. (1981). Rock Characterization Testing and Monitoring. International Society for Rock Mechanics Suggested Methods. Brown, E.T. (Ed.), Pergamon Press, Oxford, 211 pp.

[24] ASTM. (1984). Standard Test Method for Unconfined Compressive Strength of Intact Rock Core Specimens, Soil and Rock, Building Stones. Annual Book of ASTM Standards 4.08, Philadelphia, Pennsylvania.